ISSN 1392-1207. MECHANIKA. Vol. 31, No. 1, 2025: 5–14

Aerodynamic Shape Optimization of Simplified Ground Vehicle (Ahmed Body) using Passive Control Devices

Ahmet ŞUMNU*, Yüksel ERASLAN**
**İskenderun Technical University, Faculty of Aeronautics and Astronautics, Department of Aerospace Engineering, 31200, Hatay, Türkiye, E-mail: ahmet.sumnu@iste.edu.tr*
***Tarsus University, Faculty of Aeronautics and Astronautics, Aerospace Engineering Department, 33400, Mersin, Türkiye, E-mail: yukseleraslan@tarsus.edu.tr (Corresponding Author)*
https://doi.org/10.5755/j02.mech.36452

1. Introduction

Energy consumption and energy saving are probably one of the most crucial issues for all scientists working in any field of engineering sciences since usable energy is limited in the World. In the field of aeronautics, a significant amount of energy consumption is arising from aerodynamic drag and friction except for deficiency considerations in propulsion systems. Similarly, automobiles are suffering aerodynamically from the air resistance force they are subjected to. Most of the fuel consumed by an automobile is based upon skin friction drag and pressure drag, where 80% of the total aerodynamic drag is composed of these drag elements depending on the external geometry of the vehicle [1]. In order to overcome these energy losses, aerodynamic shape optimization studies have been performing to increase the aerodynamic performances of such devices. However, some design constraints do not allow for further decrease of aerodynamic drag of the vehicles even though the shape optimization is applied. Further drag reduction could be achieved possibly by applying active or passive flow control devices that arrange the flow over the vehicles. Therefore, aerodynamic optimization of vehicle geometries utilizing active or passive control devices comes to the fore in obtaining minimized energy consumption.

Active flow control devices (jet vectoring, force actuators etc.) simply bases on addition of auxiliary power into the airflow, while passive flow control devices (turbulators, roughness elements etc.) not require any energy by definition [2]. The potential behind the passive control techniques should be considered within the scope of controlling the pressure and regulating the drag force around a body. In that context, the Ahmed body is a well-known standardized vehicle geometry having adequate experimental data to compare the aerodynamic performance effects of the application of such flow control devices [3].

Passive control devices have widely been used, assessed, and investigated in many studies in the literature via analytical, numerical or experimental methods. Aider et al. performed an experimental study that placed cylindrical roughness elements on the rear of the Ahmed body model to prevent flow separation and reduce drag force, which resulted in drag reduction about 10% once the roughness elements were placed optimally [4]. Pastoor et al. used the Ahmed body by making curve rear part [5]. Vortex generators were applied as both active and passive. It was shown that the reduction of circulation of the trailing vortices could pro-vide drag reduction even early separation of flow occurs. Bayındırlı et al. performed control flow study to postpone vortex generation using feedback controller [6]. D-shaped model was used to investigate the turbulence flow and shown interplay shear layer and wake dynamics, where drag reduction was achieved about 15%. Kohri et al. applied passive control device for a bus to reduce drag that originated from pressure [7]. The results showed that drag coefficient reduced about 5.27% and this improvement also provided to reduce in fuel consumption about 3%. Thacker et al. investigated unsteady flow behaviour on the rear upper part of Ahmed body [8]. It was found that the relationship between the slant angle and Strouhal number, where this phenomenon also discussed. Viswanathan et al. proposed a study to control the flow at the rear of the Ahmed body with 25-degree slant angle [9]. Sharp and rounded edge on the roof/rear slant model was used to observe the flow physics. When compared these two methods, drag level was reduced about 10% without flow separation on the rear window. Selvaraju et al. performed flow control to improve aerodynamic performance for the Ahmed body using various VGs that are delta-winglet (DVGs), the cylindrical (CVGs) and trapezoidal (TVGs) [10]. Joseph et al. proposed empirical and numerical study to reduce drag force on a SUV car model. The study was indicated that the position of VGs was crucial aerodynamic efficiency point of view [11].

Flow separation can be suppressed or delayed using active flow control devices as well as foresaid passive devices. For example, the study that related with active flow control was proposed by Metka et al. to reduce drag force on rear slant of the Ahmed body [12]. In the study, flow of the rear end of model was controlled using pulsed jets with four different configurations. The wind tunnel test results shown that the obtained drag reduction was measured about 6-8% for different jet configurations. Another similar study that investigated flow control of the Ahmed body with rear slant angle 25-degree was presented using fluidic oscillators by Wang et al. [13]. The drag force reduction was achieved about 7% by controlling flow on the rear part of model. Yagiz et al. were also investigated bluff body with 25-degree slant angle to control flow using traditional synthetic jet [14].

On the other hand, optimization techniques are commonly used to find best results for specific problems by the designers or engineers as mentioned before. For instance, Han et al. presented a study to minimize drag using control devices and applying optimization technique [15]. Optimization was performed using gradient-based technique for 2D bump parameters of Rae5243 airfoil and the results shown that total drag reduced about 3.94% and lift

increased about 5.03%. Another similar optimization problem was solved by Karthik et al. [16]. The actuation parameters of active control device were optimized using simulated annealing Genetic algorithm. It was concluded that lift of airfoil increased about 16.9% while drag reduced about 13.4% for corresponding angle of attack. Dickison et al. studied optimization of wavy cylinder to reduce aerodynamic drag using Particle Swarm Optimization (PSO) method [17]. Ahmed et al. presented an aerodynamic optimization study for sports car [18]. The aerodynamic performance was investigated front, middle and rear region of car and modification was performed to improve drag and lift coefficients value.

The flow separation or adverse pressure gradient well known to cause drag force. For a ground vehicle, the most of the drag occurs at the rear end of body since flow separation is generally observed at that region. In literature, there is few studies related with both numerical analysis of the Ahmed body with passive control and shape optimization concurrently. Therefore, the main aim of this study is to reduce drag force by controlling the flow at rear region of the Ahmed body using passive control devices and applying shape optimization for performance improvement simultaneously.

In this paper, passive flow control over the Ahmed body to suppress or delay separation was performed using cylindrical roughness elements, and rectangular shaped VGs. The original Ahmed body is revised with addition of the foresaid passive control devices located at the rear side of the vehicle. Parametrical definitions of the devices were made in terms of distance from each other, height, width, and location with respect to the rear end. Computational Fluid Dynamics (CFD) investigation process was conducted to have aerodynamic performance assessment of various geometrical scenarios, which includes mesh independence analyses to ensure the accuracy of the results. Furthermore, the validation of the CFD analysis method carried out with the existing experimental data from the literature. Aerodynamic optimization of the Ahmed body within the limits of the determined parameters of the control devices was performed using a genetic algorithm on DesignXplorer in ANSYS.

2. Material and Method

2.1. Simplified ground vehicle and passive control device geometries

The Ahmed body has been a well-known geometry used as a simplified ground vehicle body that presented by Ahmed et al. [3]. The model was used by the authors to analyse the time average wake structure experimentally and shown that most of the drag force stemmed from the pressure difference that occurs on the rear end of the body, whose solid model is generated on ANSYS Design modeler and given with dimensions Fig. 1 and Fig. 2.

In this study, flow control over the Ahmed body to suppress or delay separation was performed using cylindrical roughness elements, and rectangular shape VGs. Cylindrical roughness elements were placed upper side of the body at three different positions and dimensions. The dimensions and array of the cylindrical roughness elements are given in Table 1 [4]. λ_z, d, and k represent the spanwise space, diameter height of roughness cylinder elements, respectively, where δ_0 is the turbulent boundary layer thickness. Rectangular shape VGs dimensions are given Table 2, where λ_z, L and H refers to distance among the VGs, length and height of VGs, respectively. The Ahmed body revised

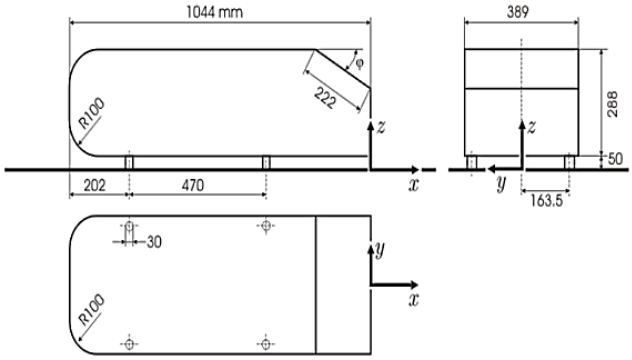

Fig. 1 Side, rear and top views of Ahmed body (dimensions in mm) [3] [19]

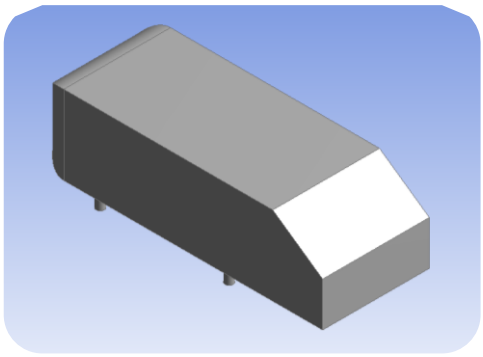

Fig. 2 The solid model of generated Ahmed body

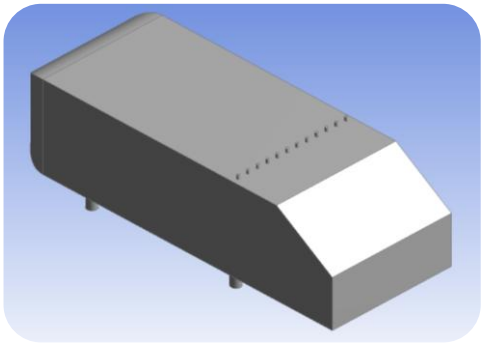

a

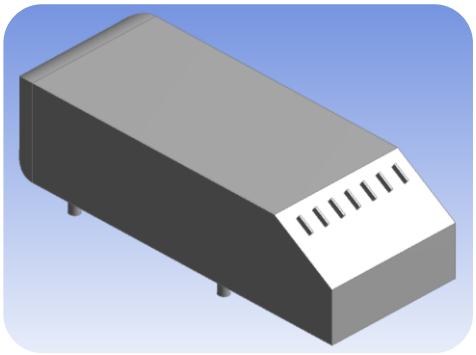

b

Fig. 3 The Ahmed body with passive control devices: a – cylindrical roughness elements, b – rectangular shape VGs

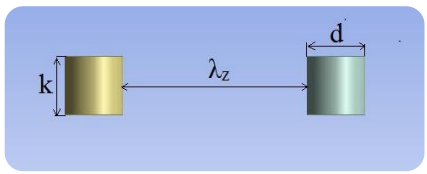

a

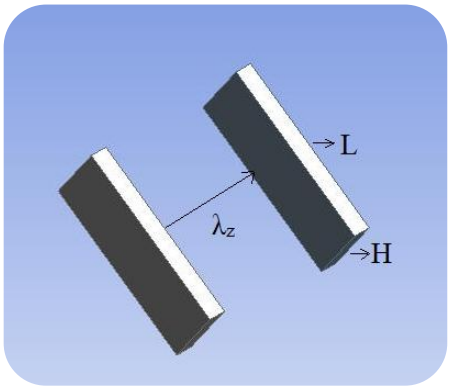

b

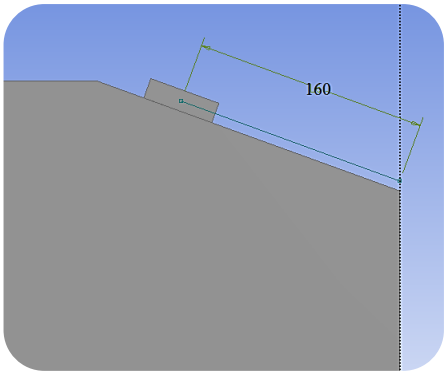

c

Fig. 4 Properties of the passive control devices on the model: a – cylindrical roughness elements, b – rectangular-shaped VGs, c – position of VGs

Table 1
Dimensions and arrays of cylindrical roughness elements [4]

Cylindrical-shaped roughness elements			
Arrangement configuration	λ_z, mm	d, mm	k/δ_0
A	24	6	0.6
B	32	8	0.6
C	48	12	0.6

Table 2
Dimensions of vortex generators

Rectangular-shaped vortex generators			
Position	λ_z, mm	L, mm	H, mm
60	50	50	20
110	50	50	20
160	50	50	20

with addition of cylindrical roughness elements and VGs are illustrated in Fig. 3.

The cylindrical roughness elements were placed on the roof of the rear region of the body and VGs were placed on the slant surface of the body since the drag force was more effective in that region due to the separation of flow. Position of the VGs were determined as the distance between the centre of the VGs and rear end of the model. The geometry and parameters of control flow devices and position of the VGs are shown in Fig. 4.

2.2. Computational fluid dynamics (CFD)

2.2.1. Mesh generation and grid independence

The mesh generation of the models were performed using ANSYS Mesher. In order to find accurate results for CFD solutions, mesh generation process was performed at several times that starts from courser to finer mesh element numbers. This process enabled to find efficient number of mesh elements for solution and avoid waste of time and reduce computational power requirement. The mesh independence chart is given in Fig. 5. The prismatic mesh structure was generated around the body to capture flow separation due to adverse pressure gradients. Mesh generation of the remaining parts of the computational domain was formed with tetrahedral mesh elements to easily generate using automatic meshing applications. Size of the computational domain in x-direction is 8 times of length of

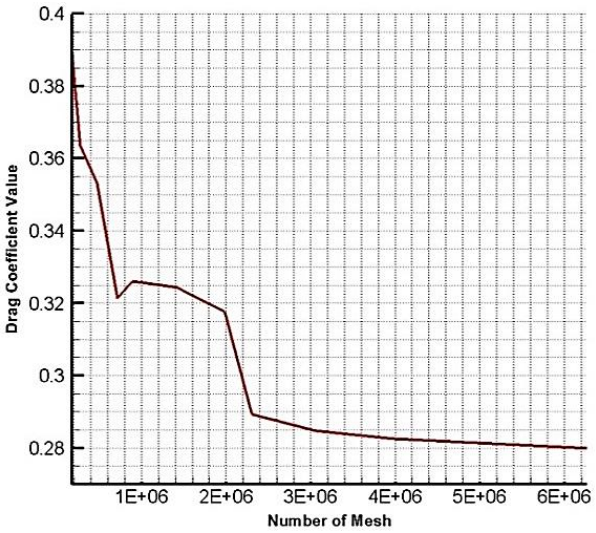

Fig. 5 Mesh (grid) independence chart for the Ahmed body [20]

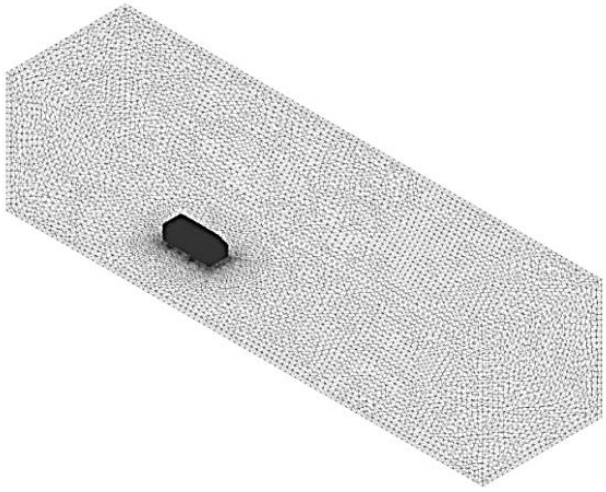

Fig. 6 Mesh structure of the computational fluid domain of the Ahmed body

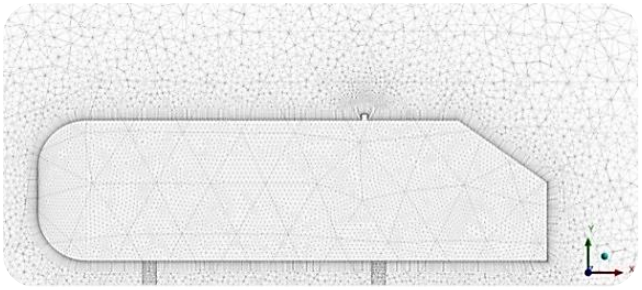

Fig. 7 Mesh structure around the Ahmed body with cylindrical roughness elements

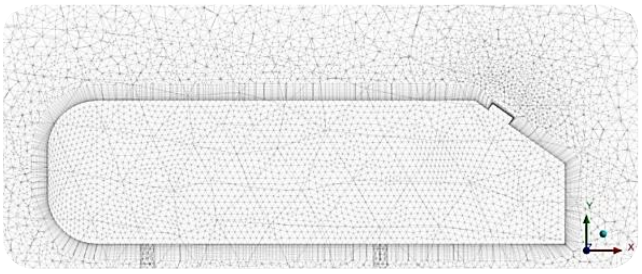

Fig. 8 Mesh structure around the Ahmed body with vortex generators

body, in *y*-direction 6 times of height of body and in z-direction 5 times of width of body. The computational fluid domain is given in Fig. 6 and generated mesh structures around the models for both of the passive control devices are given in Fig. 7 and 8.

2.2.2 Computational setup and solution

Computational Fluid Dynamics (CFD) applications are crucial in assessing and designing virtual prototyping of various engineering cases involving fluids. In this study, a Navier-Stokes solver, ANSYS Fluent, is used to investigate the Ahmed body together with various passive control devices.

Navier-Stokes equations represent the motion of a fluid element and the general governing equations of the fluid dynamics. The equations consist of the momentum, energy and continuity equations, which are used to solve the control volume elements. Furthermore, Reynolds-Averaged Navier-Stokes (RANS) equations take the viscous effects into account in a simpler way to provide convenience in solution of complex flows [21]. RANS equations can be defined for a turbulent, viscous and compressible flow in x-direction as given in following Eq. (1) to Eq. (4) [22]. The time averaging is expressed as:

$$\overline{f} = \lim_{T\to\infty} \frac{1}{T} \int_0^T f(x_i, t)dt \,. \tag{1}$$

The sum of the mean and fluctuating components can be expressed as:

$$p_i = \overline{p}_i + p' \,, \tag{2a}$$

$$u_i = \overline{u}_i + u_i' \,. \tag{2b}$$

Reynolds Averaged Navier-Stokes equations are defined as:

$$\frac{\partial \rho}{\partial t} + \frac{\partial \left(\rho \overline{u}_i\right)}{\partial x_i} = 0 \,, \tag{3}$$

$$\frac{\partial \left(\rho \overline{u}_i\right)}{\partial x_i} + \frac{\partial \left(\rho \overline{u}_i \overline{u}_i\right)}{\partial x_j} = -\frac{\partial \overline{p}}{\partial x_i} + \\ + \frac{\partial}{\partial x_j}\left[\mu\left(\frac{\partial \overline{u}_i}{\partial x_j} + \frac{\partial \overline{u}_j}{\partial x_i} - \delta_{ij}\frac{\partial \overline{u}_m}{\partial x_m}\right)\right] + \frac{\partial}{\partial x_j}\left(-\rho \overline{u_i} \overline{u}_j\right) . \tag{4}$$

As the analytic solution for the full (3-D) Navier-Stokes equations does not exist due to the complexity of partial differential equations; some assumptions could be to achieve the approximate numerical and viscous solution of the flow. The finite volume method (FVM) evaluates partial differential equations in the form of algebraic equations [23]. In finite volume method, the computation is performed in a small volume which surrounds each node point on a grid. The conservation of mass, momentum and energy can be rearranged to use solving a problem for CFD in ANSYS Fluent that uses finite volume method to solve the conservation equations. Eq. (5) represents the summarized equation for CFD solutions [24].

$$\frac{\partial}{\partial t}\overline{U} + \frac{\partial}{\partial x}\overline{F} + \frac{\partial}{\partial y}\overline{G} + \frac{\partial}{\partial y}\overline{H} = 0 \,. \tag{5}$$

$\overline{F}$, $\overline{G}$ and $\overline{H}$ are the flux terms and $\overline{U}$ is the solution vector, whose elements (ρ, ρu, ρv, ρw, ρE) are dependent variables that are acquired in steps of time. Drag coefficient that is used to determine performance of vehicles is expressed by its drag force as given in the following equation, Eq. (6).

$$C_D = \frac{D}{0.5\rho V_\infty^2 S} \,. \tag{6}$$

The terms C_D, and D are the drag coefficient and drag force, ρ, V_∞ and S are air density, free-stream velocity and cross-sectional area, respectively in Eq. (6). In the present study, the computation is performed at different free-stream velocity and slant angles of the Ahmed body with the afore-mentioned passive control devices. For the solutions, a three-dimensional, steady-state and density-based solver is defined and RNG (Re-Normalisation Group) k-ε turbulence model is used. The near wall treatment that determines non-dimensional y+ value is selected as Enhanced wall treatment since this function gives reasonable results for fine meshes and uses two-layer model as a near wall model that resolves the whole boundary layer in the viscous sublayer [25]. For the solution method, implicit formulation with Roe-FDS flux type is defined and second order upwind is selected for flow, kinetic energy and specific dissipation rate. In addition, Green-Gauss cell based is used for spatial discretization gradient operator because it provides good results for second order finite volume method. Courant number which is a dimensionless number shows the time a particle stays in cell of mesh and its value is defined as 0.7-1 for all solutions. To find the correct solution, the solution is completed when the change of CD value is lower than 1% for the last 100 iterations.

3. Results and Discussion

3.1. CFD analysis results and discussion

CFD solution of the Ahmed body with passive control devices was performed using cylindrical roughness elements, and rectangular-shaped VGs. The results were firstly given for cylindrical roughness elements placed on top of the rear region of the body with three different configurations and slant angles at 20-degree, 25-degree and 35-degree at 20 m/s airspeed. The streamlines of the flow field are visually presented in Fig. 9. The results stated that the centre of the vortex formation was delayed in x-direction for all of the configurations, and that is provided reduction in drag force due to the adverse pressure gradient. The flow separation and vortex formation can be observed on the slant surface of the model when the slant angle increases to 25-degree. 25-degree slant angle shown that the vortex formation on the slant surface was not suppressed completely however; it was delayed in the x-direction of the rear region of the model. Hence, it can be concluded that the applied control devices have indicated positive effect in terms of aerodynamics by means of suppressing and delaying flow separation. However, the recirculation bubble has not been suppressed on the slant surface for the configuration C. The velocity streamlines of the Ahmed body with VGs for base model and three different positions are presented in Fig. 10. It is clear from the figure that the size of the vortex occurring on the rear region of base model was larger than model with VGs and centre of vortex was also delayed. In addition, when the size of the vortex compared, VGs placed at 60 mm is resulted in smaller than others. In order to show effectiveness of VGs, CFD analysis was also performed at 25-degree and 35-degree slant surface of the body. When the figure examined, VGs found to be prevented the flow separation and reduce adverse pressure gradient for especially when placed at 110 and 60 mm. The formation of vortices occurred on the slant surface of the body and caused the increase of drag force. By means of used VGs, low separation and vortex formation on slant surface were suppressed and prevented. Moreover, vortex size occurring rear region of the model decreased for slant surface of model at the 35-

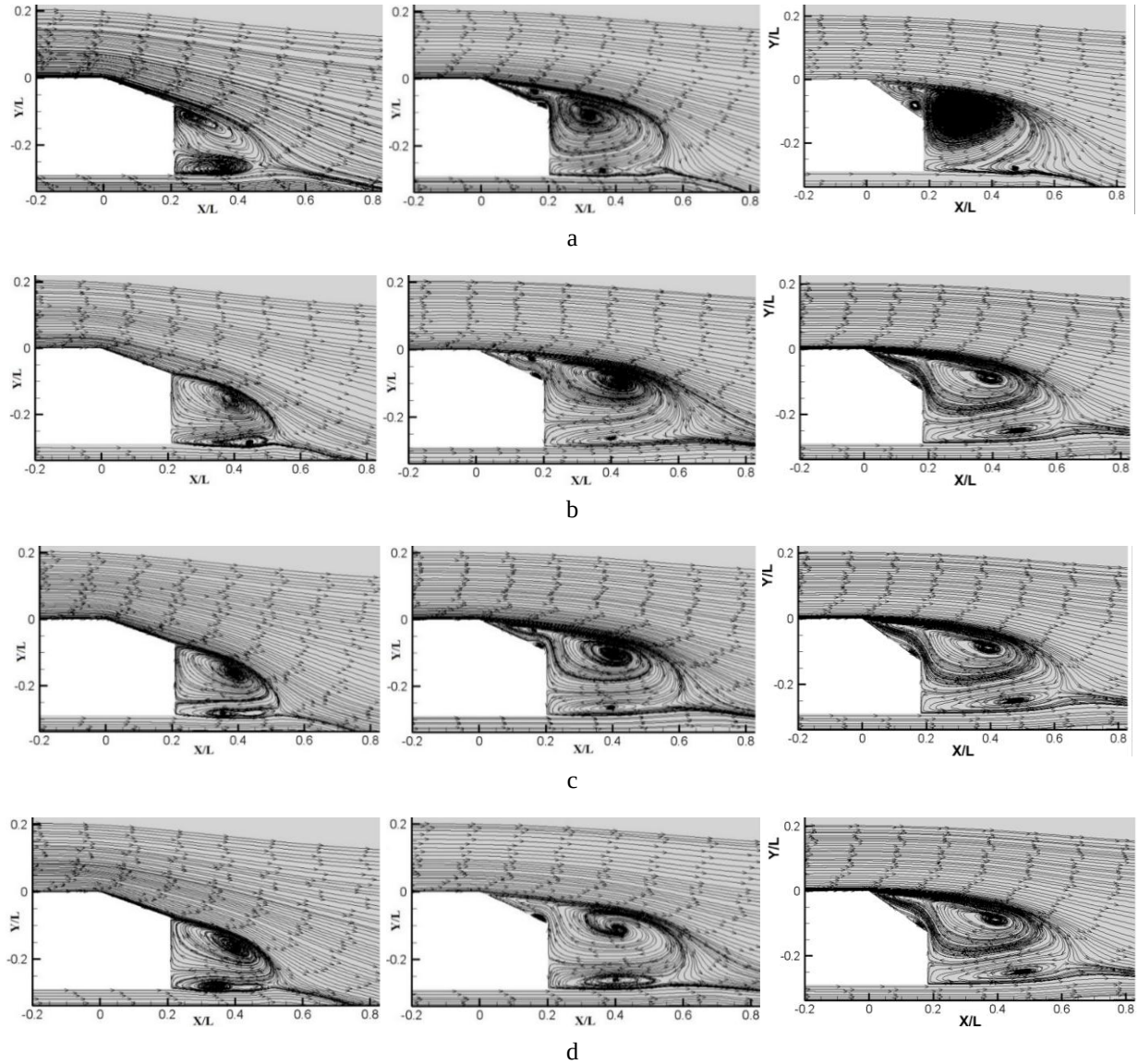

Fig. 9 Velocity streamlines or velocity contours at 20 m/s airspeed: a – base model (left), 20° slant angle (middle) and 35° slant angle (right), b – configuration A with base model (left), 20° slant angle (middle) and 35° slant angle (right), c – configuration B with base model (left), 20° slant angle (middle) and 35° slant angle (right), d – configuration C with base model (left), 20° slant angle (middle) and 35° slant angle (right)

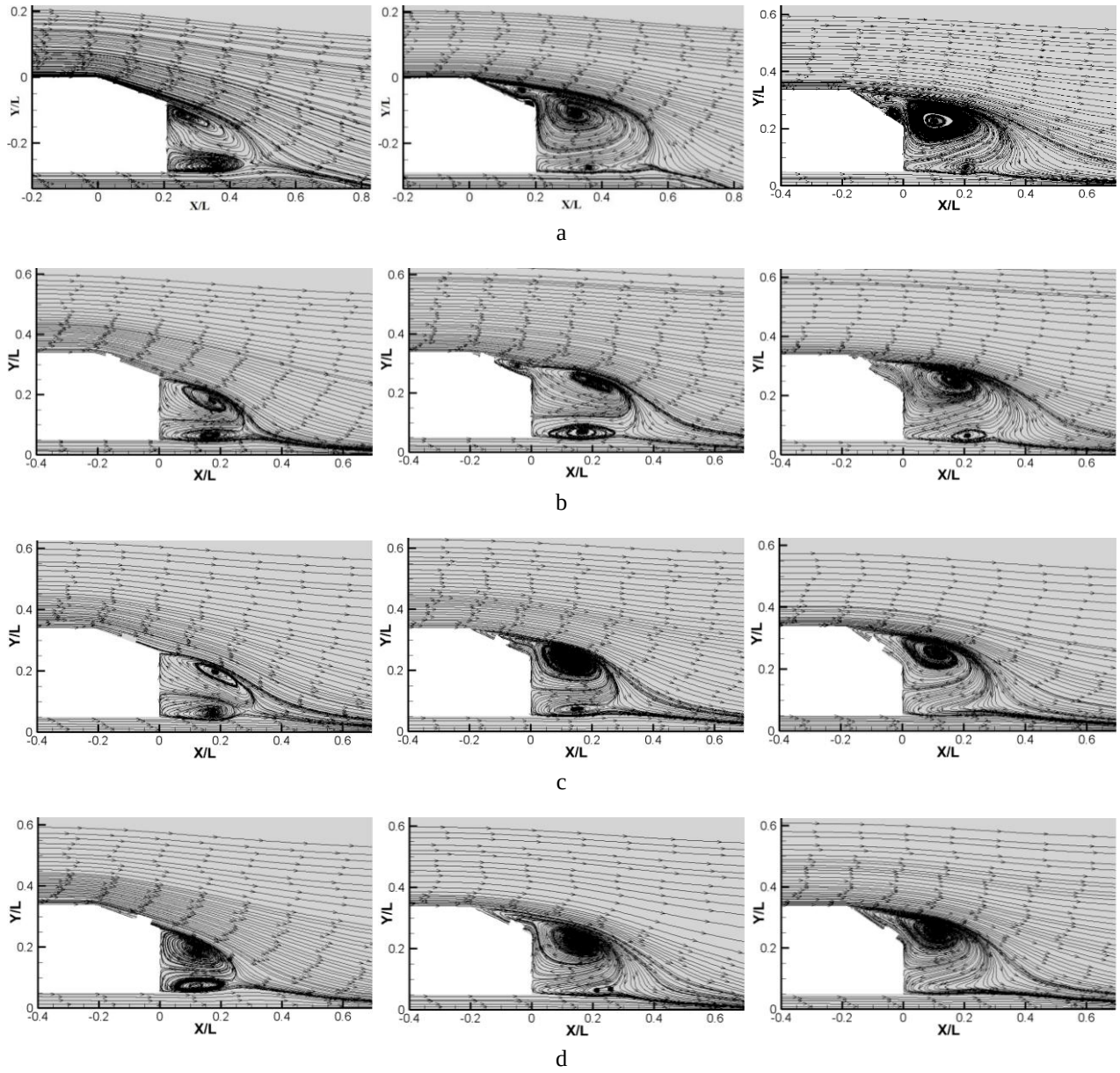

Fig. 10 Velocity streamlines or velocity contours at 20 m/s airspeed: a – base model (left), VGs placed at 60 mm (middle) and VGs placed at 60 mm (right), b – base model with 20° slant angle (left), VGs placed at 160 mm (middle) and VGs placed at 60 mm (right), c – base model with 25° slant angle (left), VGs placed at 110 mm (middle) and VGs placed at 60 mm (right), d – base model with 35° slant angle (left), VGs placed at 60 mm (middle) and VGs placed at 60 mm (right)

degree with VGs. In conclusion, the use of VGs shown especially superior performance aerodynamics point of view for slant surface 35-degree.

3.2. Aerodynamic shape optimization

3.2.1. Genetic algorithm

Genetic algorithm (GA) is a type of Evolutionary Algorithm (EA) widely used in finding optimum solution for engineering problems. GA is a heuristic scanning method developed inspired by the change processes in nature. It is a robust and flexible approach in general and can be used to solve many problems with both discrete and continuous character [26].

In the optimization problem, firstly, the objective function should be defined and later on the population should be specified. The upper and lower limit for the solution of a problem can be defined when there may not be idea for some problem. Every individual in the population can be generated by the random number operator as following Eq. (7) [27].

$$x_{i,j}^{(0)} = x_j^L + \left(x_j^U - x_j^L\right) rand\,(0,1)\,, \tag{7a}$$

$$i = 1,2,...,N_p\,, \tag{7b}$$

$$j = 1,2,...,n\,, \tag{7c}$$

where x_i represents the i. chromosome in the population, $x_{i,j}$ represents the j. gene of chromosome, n is the gene number and N_p indicates population size $x_j^U - x_j^L$ indicates the upper and lower limits of gene. If the designers have a

knowledge about the solution of the problem, the initial population can be selected that is closer the optimal solution. The concept of Elitism transfers the best solution from generation to generation and this provides to find fitness value. Elite individual update in each generation can be performed according to the following Eq. (8) and (9) [27].

$$f^{el}(t) = \arg\min_{f_i(t)} f\left(x_i(t)\right), \tag{8}$$

$$x^{el}(t) = \begin{Bmatrix} x^{el}(t-1) & f^{el}(t) > f^{el}(t-1) \\ x^{el}(t) & f^{el}(t) \le f^{el}(t-1) \end{Bmatrix}, \tag{9}$$

where t is generation number, $f^{el}(t)$ is the objective function value of elitism individual and $x^{el}(t)$ is the design vector.

The selection process of GA is performed by selecting individual genomes from population to use crossover process. The crossover of two parent string produces offspring by changing genes of the chromosomes. In crossover process, the individual number can be specified Eq. (10).

$$N_s = N_p\left(1 - P_c\right), \tag{10}$$

where N_s is the individual number for crossover, P_c is crossover rate. Then, individual number with crossover can be obtained Eq. (11).

$$N_c = N_p P_c . \tag{11}$$

Mutation process that is widely used genetic operator provides genetic diversity from one generation of population of genetic algorithm chromosomes to the next. The number of genes that applies mutation process can be defined as given in Eq. (12).

$$G_m = nR_m\left(N_p - N_e\right), \tag{12}$$

where G_m is the gene number and R_m is the mutation rate.

3.2.2. Design of experiments

The aim of the design of experiments (DoE) is to gather set of data to calculate a response surface that is used to run an optimization for a response surface optimization. In the DoE step, the design space is explored and the test matrix of design points are generated to investigate each computational experiment. Box-Behnken Design algorithm is used to generate the design points due to its advantages of understanding the potential interactions between parameters and saving process time by reducing the number of experiments [28].

3.2.3. Response surfaces

Response surface describes the output parameters in terms of the input parameters, and can provide the approximated values of the output parameters analysed in design space without obtaining complete solution. Genetic aggregation and Kriging Response Surface types are commonly used to analyse design space. Genetic Aggregation is used when dealing with high number of design points while Kriging type is efficient in a large number of cases and it is suitable for highly nonlinear responses. Hence, in this study, Kriging type is used to analyse Response Surface since it gives more accurate results for nonlinear responses.

3.2.4. Optimization solution, results and discussion

The optimization is carried out to find the optimum sizes of passive control devices by means of DesignXplorer in ANSYS. The first step of the optimization process is determination of the objective and design parameters for both devices. The objective of this study is reduction in drag force and design parameters for cylindrical roughness elements are height (k) and diameter (d) of the elements. The cylindrical roughness elements are placed at the optimal streamwise position that is found between $4\lambda_z$ and $5\lambda_z$ upstream of the separation line [4]. The passive control elements are positioned about $4.5\lambda_z$ for three configurations. In addition, λ_z, L and H are defined as the design parameters for rectangular-shaped VGs. Design points should be generated to start the optimization, where nine and thirteen different design points are determined for cylindrical roughness elements and rectangular-shaped VGs, respectively. Later on, CFD analysis is performed for each to obtain optimal solution, within some determined constraints given with the equations below.

$$C_{D_{opt}} < C_{D_{base}} , \tag{13}$$

$$k_{cyd}^{L} < k_{cyd} < k_{cyd}^{U} , \tag{14}$$

$$d_{cyd}^{L} < d_{cyd} < d_{cyd}^{U} . \tag{15}$$

The upper and lower limits for cylinder heights of roughness elements are defined as k_{cyd}^{L} and k_{cyd}^{U}, which are $\mp$10% of the base height. Moreover, diameter limits of the cylinders are defined as d_{cyd}^{L} and d_{cyd}^{U}, which are $\mp$10% of the base diameter.

$$x_j^{U} - x_j^{L} , \tag{16}$$

$$L_{VGs}^{L} < L_{VGs} < L_{VGs}^{U} , \tag{17}$$

$$H_{VGs}^{L} < H_{VGs} < H_{VGs}^{U} . \tag{18}$$

The upper and lower limits for the length and height of VGs are defined as L_{VGs}^{L}, H_{VGs}^{L}, L_{VGs}^{U} and H_{VGs}^{U}, which are $\mp$10% of their base values. In addition, VG position limits are defined as P_{VGs}^{L} and P_{VGs}^{U}, which are $\mp$20% of the base spanwise space.

Optimization solution is performed for three different configurations at 35-degree slant angle and 20 m/s free-stream velocity. The response surfaces are presented for each configuration in Fig. 11, Fig. 12 and Fig. 13. The figures shown the variation of objective variable (drag force) with design variables (diameter and height). Fig. 11 indicates that the diameter of control device was more effective than its height. The Fig. 12 shown that the increase of both design variables is dramatically increased the drag force.

Moreover, Fig. 13 is clearly illustrated similar characteristics with Fig. 12. In summary, drag force is found to be increased with the increase in the both design variables. However, the decrease in size of the design variables found to be resulted in a sudden reduction in drag force. Hence, its optimum results are closer to that point.

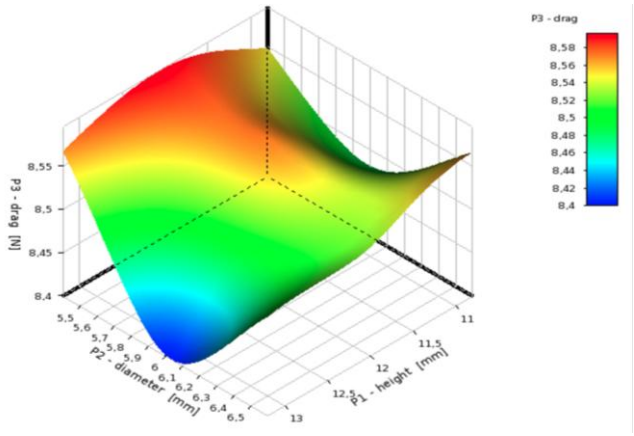

Fig. 11 Response surface for configuration A

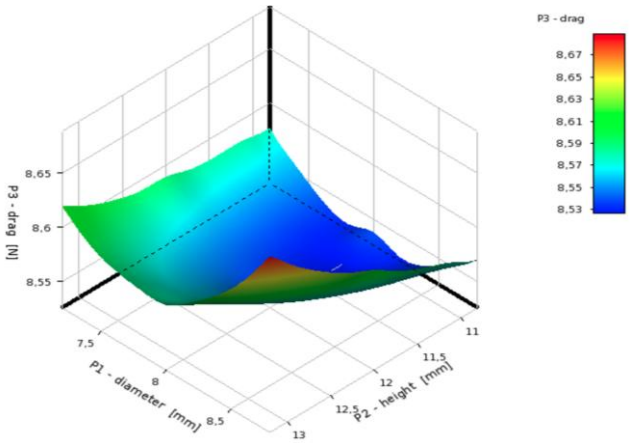

Fig. 12 Response surface for configuration B

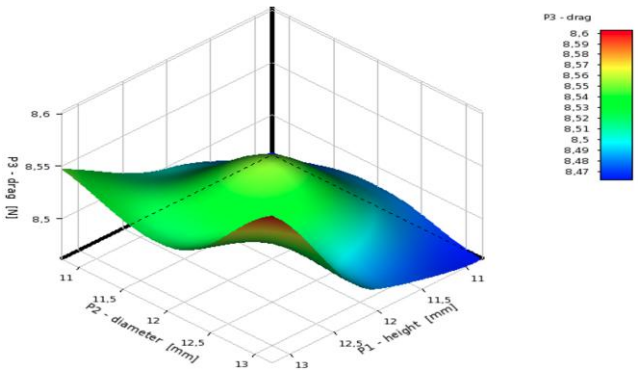

Fig. 13 Response surface for configuration A

Optimization processes are also carried out for obtaining optimum shape of VGs. In order to show sensitivity between the design parameters of VGs, response surface chart is given in Fig. 14-16. When Fig. 14 is examined, the increase of length of VGs reduces the drag force if the length is higher than 48 mm while increase of its height adversely effects the aerodynamic performance. The similar case can be stated for the Fig. 16 that shows length versus VGs position. When VGs position is closer to end of slant surface, drag force is adversely affected. The other response surface chart is Fig. 16 that represents the relation between VGs position and its height, where can be concluded that the change of drag force is further for the VGs height. Therefore, the optimum case can be observed when VGs height is reduced together with its position is placed towards top of the slant

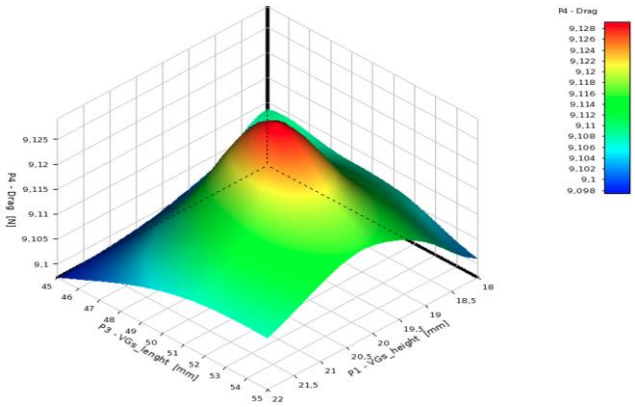

Fig. 14 Response surface for VGs length versus height

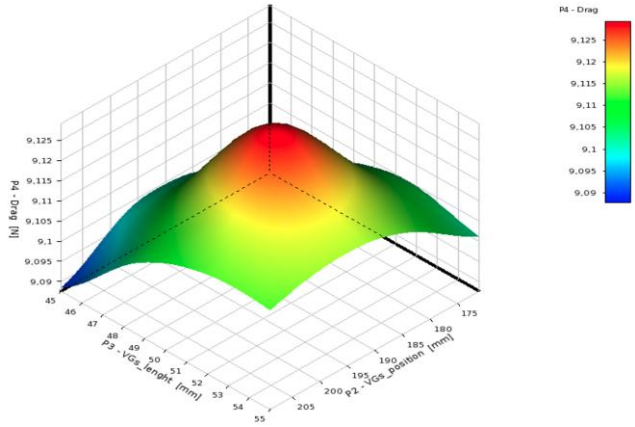

Fig. 15 Response surface for VGs length versus its position

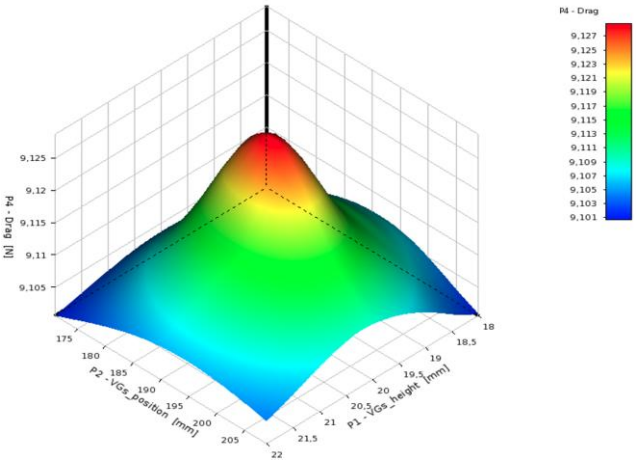

Fig. 16 Response surface for VGs position versus height surface

The results of the optimization solution for objective variable are given in Table 4. Results of design variable for each cylindrical roughness elements configurations and VGs are given in Table 5 and 6, respectively.

Table 4
Results of objective variables for each configuration of cylindrical roughness elements and VGs

Objective Variable		$C_{D_{base}}$	$C_{D_{opt}}$
Cylindrical Roughness Element	A	0.2719	0.2638
	B	0.2698	0.2597
	C	0.2807	0.2681
Vortex Generators		0.2606	0.2501

Table 5
Results of design variables for each configuration of cylindrical roughness elements

Design Variable, mm	A	B	C
k_{base}	12	12	12
$k_{optimum}$	12.72	11.185	10.801
d_{base}	6	8	12
$d_{optimum}$	5.85	7.92	10.801

Table 6
Results of design variables for VGs

Design Variable	Value, mm
H_{base}	20
$H_{optimum}$	18.13
L_{base}	50
$L_{optimum}$	54.87
Base position	110
Optimum position	118.77

3. Conclusions

This study aims to control the flow around the Ahmed body thanks to coherent streamwise streaks by suppressing or delaying the separation that occur rear end of model due to adverse pressure gradient. For that purpose, two different passive control devices, which are cylindrical roughness elements and VGs, were used and an optimization process was performed to find optimum aerodynamic shapes and locations of the devices. Firstly, validation process of the numerical simulation was performed, and later on CFD analyses were performed to solve the flow field for Ahmed body combined with application of various configurations of cylindrical roughness elements and VGs. In conclusion of the CFD analyses, the flow separation on rear region of the model was found to be delayed and it was stated that drag coefficient reduced thanks to the delayed vortex centre and prevented the vortex formation on the slant surface of the model.

On the other hand, aerodynamic shape optimization of the devices was performed with generated nine and thirteen design points for cylindrical elements and VGs, respectively. The process was carried out using Genetic Algorithm, and in conclusion, the drag coefficient reduced about 3.02%, 3.76% and 2.58% for A, B and C configurations of cylindrical roughness elements, and 4.21% for VGs, respectively. The results of optimization also shown that separation of flow of rear end of model was delayed and that total drag reduction was achieved about 8.23% and 11.62% with optimum shape of cylindrical roughness elements and rectangular-shaped VGs, respectively.

In conclusion, this study proposes a remarkable drag reduction and correspondingly improved fuel efficiency for automobiles via application of passive control devices. Such applications commonly applied on racing cars while application of these devices on city cars could have difficulties in leading to an additional cost, requirement for maintenance and various aesthetic concerns. However, the designer should certainly carry out a tradeoff within the benefits in fuel-efficiency, stability and noise reduction before an application.

References

1. **Mukut, A. M. I.; Abedin, M. Z.** 2019. Review on Aerodynamic Drag Reduction of Vehicles, International Journal of Engineering Materials and Manufacture 4(1): 1-14. https://doi.org/10.26776/ijemm.04.01.2019.01.
2. **Joshi, S. N.; Gujarathi, Y. S.** 2016. A Review on Active and Passive Flow Control Techniques, International Journal on Recent Technologies in Mechanical and Electrical Engineering 3(4): 1-6.
3. **Ahmed, S. R.; Ramm, G.; Faltin, G.** 1984. Some Salient Features Of The Time-Averaged Ground Vehicle Wake, SAE transactions 473-503.
4. **Pujals, G.; Depardo S.; Cossu, C.** 2010. Drag reduction of a 3D bluff body using coherent streamwise streaks, Experiments in fluids 49: 1085-1094. https://doi.org/10.1007/s00348-010-0857-5.
5. **Aider, J. L.; Beaudoin, J. F.; Wesfreid, J. E.** 2010. Drag and lift reduction of a 3D bluff-body using active vortex generators, Experiments in fluids, 48: 771-789. https://doi.org/10.1007/s00348-009-0770-y.
6. **Pastoor, M.; Henning, L.; Noack, B. R.; King, R.; Tadmor, G.** 2008. Feedback shear layer control for bluff body drag reduction, Journal of Fluid Mechanics 608: 161-196. https://doi.org/10.1017/S0022112008002073.
7. **Bayındırlı, C.; Çelik, M.; Demiralp, M.** 2018. Bir otobüs modeli etrafındaki akış yapısının CFD yöntemi ile incelenmesi ve sürükleme kuvvetinin pasif akış kontrol yöntemi ile iyileştirilmesi, Politeknik Dergisi 21(4): 785-795. https://doi.org/10.2339/politeknik.403993.
8. **Kohri, I.; Yamanashi, T.; Nasu, T.; Hashizume, Y.; Katoh, D.** 2014. Study on the Transient Behaviour of the Vortex Structure behind Ahmed Body, SAE International Journal of Passenger Cars-Mechanical Systems 7(2014-01-0597): 586-602. https://doi.org/10.4271/2014-01-0597.
9. **Thacker, A.; Aubrun, S.; Leroy A.; Devinant, P.** 2012. Effects of suppressing the 3D separation on the rear slant on the flow structures around an Ahmed body, Journal of Wind Engineering and Industrial Aerodynamics 107-108: 237-243. https://doi.org/10.1016/j.jweia.2012.04.022.
10. **Viswanathan, H.** 2021. Aerodynamic performance of several passive vortex generator configurations on an Ahmed body subjected to yaw angles, Journal of the Brazilian Society of Mechanical Sciences and Engineering 43(3): 131. https://doi.org/10.1007/s40430-021-02850-8.
11. **Selvaraju, P. N.; Parammasivam, K. M.** 2019. Empirical and Numerical Analysis of Aerodynamic Drag on a Typical SUV Car Model at Different Locations of Vortex Generator, Journal of Applied Fluid Mechanics 12(5): 1487-1496. https://doi.org/10.29252/jafm.12.05.29674.
12. **Joseph, P.; Amandolese, X.; Aider, J. L.** 2012. Drag

reduction on the 25° slant angle Ahmed reference body using pulsed jets, Experiments in fluids 52: 1169-1185. https://doi.org/10.1007/s00348-011-1245-5.
13. **Metka, M.; Gregory, J. W.** 2015. Drag Reduction on the 25-deg Ahmed Model Using Fluidic Oscillators, ASME Journal of Fluids Engineering 137(5): 051108. https://doi.org/10.1115/1.4029535.
14. **Wang, B. X.; Yang, Z. G.; Zhu, H.** 2019. Active flow control on the 25° Ahmed body using a new unsteady jet, International Journal of Heat and Fluid Flow 79: 108459. https://doi.org/10.1016/j.ijheatfluidflow.2019.108459.
15. **Yagiz, B.; Kandil O.; Pehlivanoglu, Y. V.** 2012. Drag minimization using active and passive flow control techniques, Aerospace Science and Technology 17(1): 21-31. https://doi.org/10.1016/j.ast.2011.03.003.
16. **Han, Z. H.; Zhang, K. S.; Song W. P.; Qiao, Z. D.** 2010. Optimization of Active Flow Control Over an Airfoil Using a Surrogate-Management Framework, Journal of Aircraft 47(2): 603-612. https://doi.org/10.2514/1.45899.
17. **Karthik, K.; Jeyakumar, S.; Sebastin, J. S.** 2021. Optimization of wavy cylinder for aerodynamic drag and aeroacoustic sound reduction using computational fluid dynamics analysis, Proceedings of the Institution of Mechanical Engineers, Part C: Journal of Mechanical Engineering Science 235(11): 1979-1991. https://doi.org/10.1177/0954406220950353
18. **Dickison, M.; Ghaleeh, M.; Milady, S.; Subbakrishna, S.; Wen, L. T.; Al Qubeissi, M.** 2020. Investigation into the aerodynamic performance of a concept sports car, Journal of Applied Fluid Mechanics, 13(2): 583-601. https://doi.org/10.29252/jafm.13.02.30179.
19. **Hinterberger, C.; García-Villalba, M.; Rodi, W.** 2004. Large eddy simulation of flow around the Ahmed body, In: McCallen, R.; Browand, F.; Ross, J. (eds) The Aerodynamics of Heavy Vehicles: Trucks, Buses, and Trains. Lecture Notes in Applied and Computational Mechanics 19: 77-87. Berlin: Springer. https://doi.org/10.1007/978-3-540-44419-0_7.
20. **Şumnu, A.** 2021. Shape modification of Ahmed body to reduce drag coefficient and determination of turbulence model, Niğde Ömer Halisdemir Üniversitesi Mühendislik Bilimleri Dergisi 10(2): 824-832. https://doi.org/10.28948/ngumuh.879584.
21. **Despirito, J.; Washington, W. D.; Vaughn, M. E.** 2004. Numerical Investigation of Aerodynamics of Canard-Controlled Missile Using Planar and Grid Tail Fins, Part II: Subsonic and Transonic Flow, Army Research Laboratory, Aberdeen Proving Ground ARL-TR-3162. 104 p.
22. ANSYS Fluent, ANSYS Fluent User's Guide. 2011. Ansys Inc.
23. **LeVeque, R. J.** 2002. Finite Volume Methods for Hyperbolic Problems. Cambridge: Cambridge University Press. 580p. https://doi.org/10.1017/CBO9780511791253.
24. **Anderson, J. D.** 1995. Computational Fluid Dynamics. New York: McGraw-Hill. 547p.
25. **Chen, H.; Patel, V.** 1988. Near-Wall Turbulence Models for Complex Flows Including Separation, AIAA Journal 26(6): 641-648. https://doi.org/10.2514/3.9948.
26. **McCall, J.** 2005. Genetic algorithms for modelling and optimization, Journal of Computational and Applied Mathematics 184(1): 205-222. https://doi.org/10.1016/j.cam.2004.07.034.
27. **Pehlivanoğlu, Y.** 2017. Optimizasyon: Temel Kavramlar & Yöntemler, Ankara, Türkiye.
28. **Yu, X. L.; He, Y.** 2017. Application of Box-Behnken designs in parameters optimization of differential pulse anodic stripping voltammetry for lead (II) determination in two electrolytes, Scientific reports 7(1): 2789. https://doi.org/10.1038/s41598-017-03030-2.

A. Şumnu, Y. Eraslan

AERODYNAMIC SHAPE OPTIMIZATION OF SIMPLIFIED GROUND VEHICLE (AHMED BODY) USING PASSIVE CONTROL DEVICES

S u m m a r y

The present study aims to control the flow separation on the simplified ground vehicle (Ahmed Body) utilizing cylindrical roughness elements and vortex generators (VG) as passive control devices. To simulate the flow over the solid body, the Computational Fluid Dynamics (CFD) method was used and combined with aerodynamic shape optimization applied concurrently to obtain the optimal dimensions and position of the passive control devices. Firstly, aerodynamic analysis methodology was validated by conducting also mesh independence study with experimental results from the literature. Later on, by changing the slant surface angle of the model, the analyses were performed to indicate different scenarios and the results were presented visually for each case. Aerodynamic shape optimization is performed using a Genetic Algorithm (GA) on DesignXplorer in ANSYS to find the optimum size and location of the passive control devices that minimize drag force, as an objective. Consequently, the flow separation of the rear end of the body was found to be delayed or suppressed and vortex height is to be reduced thanks to the applied passive control devices. The total drag reduction was achieved by about 8.23% and 11.62% for the optimal shape and location of the cylindrical roughness elements and VG devices, respectively, comparing to the baseline model.

Keywords: aerodynamics, computational fluid dynamics, ground vehicle, optimization.

Received February 25, 2024
Accepted February 21, 2025